Single-mode tapered quantum cascade lasers

Cite as: Appl. Phys. Lett. **102**, 181102 (2013); https://doi.org/10.1063/1.4804261
Submitted: 22 March 2013 . Accepted: 22 April 2013 . Published Online: 06 May 2013

Patrick Rauter, Stefan Menzel, B. Gokden, Anish K. Goyal, Christine A. Wang, Antonio Sanchez, George Turner, and Federico Capasso

Single-mode tapered quantum cascade lasers

Patrick Rauter,[1] Stefan Menzel,[1] B. Gokden,[1] Anish K. Goyal,[2] Christine A. Wang,[2] Antonio Sanchez,[2] George Turner,[2] and Federico Capasso[1,a)]
[1]*School of Engineering and Applied Sciences, Harvard University, 29 Oxford St., Cambridge, Massachusetts 02138, USA*
[2]*MIT Lincoln Laboratory, 244 Wood St., Lexington, Massachusetts 02420, USA*

(Received 22 March 2013; accepted 22 April 2013; published online 6 May 2013)

We demonstrate tapered quantum cascade lasers monolithically integrated with a distributed Bragg reflector acting as both a wavelength-selective back mirror and a transverse mode filter. Each of the 14 devices operates at a different wavelength between 9.2 and 9.7 μm, where nine devices feature single-mode operation at peak powers between 0.3 and 1.6 W at room temperature. High output power and excellent beam quality with peak brightness values up to 1.6 MW cm^{-2} sr^{-1} render these two-terminal devices highly suitable for stand-off spectroscopy applications. © *2013 AIP Publishing LLC*. [http://dx.doi.org/10.1063/1.4804261]

For numerous sensing and spectroscopy applications, quantum cascade lasers (QCLs[1–3]) are the ideal source of mid-infrared radiation. The use of QCLs as a flexible and convenient source for stand-off spectroscopy applications[4] has been increasing the need for tunable high-power, single-mode devices, a demand which has up to now been mostly fulfilled by external-cavity (EC) QCLs.[5] In the latter, the emission wavelength of a broadband QCL is selected by providing feedback from an external grating. EC QCLs allow continuous tuning of the emission wavelength over the gain spectrum by rotating and translating this grating. As an alternative approach for spectroscopy applications, arrays of single-mode QCLs[6,7] covering a series of discrete wavelengths in the targeted spectral region can serve as a multi-wavelength source with no moving parts. However, conventional distributed feedback (DFB) QCLs as single-mode elements of an array have up to now been limited in their peak power and power uniformity from device to device. In order to achieve the power increase required for stand-off spectroscopy systems by implementing broad area devices, strategies for maintaining a good beam quality are required. Very recently, arrays of DFB QCLs monolithically integrated with tapered optical amplifiers in master-oscillator power-amplifier (MOPA) configuration have made high peak power accessible for single-mode operation with excellent beam quality at a series of wavelengths.[8,9] However, while the disadvantage of EC QCLs lies in the mechanical nature of the tuning mechanism, MOPA arrays and other tunable sources based on multi-section devices[10–12] require a more complex electronic setup for independent driving of the individual device sections. Very recently, two different approaches for two-terminal broad area QCLs capable of high-power operation and good beam quality have been demonstrated. The angled cavity QCLs reported in Ref. 13 are capable of several Watts of output power under single-mode operation, while the high-brightness multi-mode QCLs demonstrated in Refs. 14 and 15 are based on a tapered Fabry-Perot cavity. The geometry of tapered QCLs allows the suppression of higher-order lateral modes, while the increase in volume of the gain material over that of conventionally designed ridge devices results in a significant increase in available peak power. While high-brightness, single-mode operation of tapered diode lasers using an integrated distributed Bragg reflector (DBR) as back mirror was demonstrated recently,[16] tapered QCLs have so far been limited to multi-mode operation at room temperature.[14,15,17] In this work, single-longitudinal and single-spatial-mode tapered QCL devices are demonstrated, where mode selection is achieved by implementing the tapered-oscillator (TO)/DBR-concept. Both the longitudinal and transverse mode filtering is performed by a narrow, monolithically integrated DBR section, leading to high peak output powers and brightness in single-mode operation by a two-terminal broad area QCL.

For the devices presented in this work, a GaInAs/AlInAs broadband bound-to-continuum heterostructure[18] grown by organometallic vapor phase epitaxy (OMVPE) on a conducting InP substrate was used. A 3.5-μm-thick, highly doped InP layer ($n = 1 \times 10^{17}$ cm^{-3}) is followed by a 520-nm-thick layer of GaInAs ($n = 3 \times 10^{16}$ cm^{-3}) and the active region composed of 35 periods of the following layer sequence (AlInAs barriers bold, GaInAs wells Roman, thickness in nm, underlined layers doped to $n = 1.5 \times 10^{17}$ cm^{-3}): **4.4**/1.7/**0.9**/5.3/**1.1**/5.2/**1.2**/4.7/**1.3**/4.2/**1.5**/3.9/**1.6**/3.4/**1.8**/3.1/**2.1**/2.8/**2.5**/2.7/**3.2**/2.7/**3.6**/2.5. After growing an additional injector sequence and 520 nm of GaInAs ($n = 3 \times 10^{16}$ cm^{-3}), the structure is completed by 3.5 μm of InP ($n = 1 \times 10^{17}$ cm^{-3}) forming the upper waveguide cladding and the top contact layer composed of 500 nm of InP ($n = 5 \times 10^{18}$ cm^{-3}) and 20 nm of GaInAs ($n = 1.8 \times 10^{19}$ cm^{-3}).

A chip of sixteen tapered oscillators with a DBR back mirror based on a buried first-order grating was realized. For the fabrication of the DBR, the InP cladding layer was removed from the grown material by wet etching in a HCl:H_2O (1:1) solution. The DBR was defined by electron-beam lithography and ion-etching into the now exposed 520-nm-thick GaInAs layer with an etch-depth of 250 nm. In order to allow the operation of each device at a different wavelength, the grating period was reduced from device to device between 1.55 μm and 1.44 μm. After etching, the InP cladding and top-contact layer sequence were regrown by

a)capasso@seas.harvard.edu

OMVPE. The geometry of the TO and DBR section was defined by reactive ion-etching of double trenches, the layout of which is presented in the inset of Fig. 1. The TO section features a tapering half-angle of 1.3° and narrows down to 13 μm at its interface with the DBR, which was in turn incorporated in a 13-μm-wide ridge. Both the TO and DBR sections are 2 mm long. Ti/Au metallization was applied as a top contact and 450-nm-thick SiN serves as an electrical insulation. The array was mounted epilayer-side up on a temperature-controlled heat sink. The facets are uncoated.

The general layout of the TO/DBR devices thus resembles that of conventional tapered lasers which comprise tapered and straight sections.[14,15,19] However, while both multi-mode TOs and TO/DBR diode lasers commonly feature an active (pumped) straight ridge-waveguide (RW) section for transverse mode filtering, the devices presented in this work operate without a pumped RW segment. The DBR directly interfaces with the tapered section and is left unpumped. The latter is enabled by electronically separating the DBR from the TO, as seen in the inset of Fig. 1. The RW section of single-mode tapered diode lasers realized up to now has been driven at a lower current density than the tapered section, requiring three terminals for driving and complicating the electronic setup. Abandoning the active RW section in the design demonstrated here allows the realization of two-terminal devices with the advantage of a significantly simplified electronics. Despite the absence of a pumped RW section in our devices in contrast to conventional tapered lasers, the strategy for suppressing higher order lateral modes remains unchanged. Modes experiencing feedback by the DBR are subject to losses in this section, where higher order lateral modes experience strong losses within the DBR section due to its narrow width and lasing at these modes is suppressed. As confirmed by the experimental results, the lateral mode filtering by the unpumped DBR section is sufficiently effective to guarantee an excellent beam quality.

The individual TO/DBR elements of the chip were characterized in pulsed operation at a heat sink temperature of 18 °C. Emission spectra were recorded using a Fourier-transform infrared spectrometer with a resolution of 0.1 cm^{-1}. Figure 2 shows an emission spectrum for each of the functional devices (two devices were not lasing due to a short), measured at a drive current pulse length of 40 ns and a repetition rate of 10 kHz. As seen in the plot, each element emits at a different wavenumber between 1031.6 cm^{-1} (device 1) and 1092.4 cm^{-1} (device 14). Six of the devices showed single-mode operation with a side-mode suppression ratio (SMSR) of at least 20 dB up to the drive current limit of the employed pulse generator of about 7 A (devices 1, 3, 4, 8, 9, and 10), reaching peak power values between 840 mW and 1.4 W. Three devices (11, 12, and 13) showed multi-mode operation at drive currents higher than those given in Fig. 2, their peak power for single-mode operation is thus limited to values between 300 and 410 mW. For five devices (2, 5, 6, 7, and 14) multi-mode operation sets in at very low currents just above threshold.

The difference in the range of single-mode operation between the individual devices is due to the mode selection conditions of the DBR/facet cavity, which vary from device to device. As reported for a MOPA array fabricated on the same chip with equivalent grating parameters,[9] the photonic bandgap of the gratings has a width of about 1.5 cm^{-1}. Due to this relatively wide DBR stopband, the roundtrip condition can be fulfilled by multiple modes for some of the array elements, leading to the observed multi-mode behaviour.

An optimization of the DBR grating in future devices is expected to give a uniform single-mode operation at high output powers for each of the elements on a chip, thus forming a tunable single-mode source highly suitable for spectroscopic applications. While switching between the individual devices of such an array allows the addressing of discrete emission wavelengths, temperature tuning of each array element either by bias-current-induced heating or by adjusting the heat sink temperature can be employed to achieve continuous spectral tunability for future, optimized TO/DBR QCL arrays. In Ref. 20, continuous tuning of the output of a DFB QCL array was demonstrated, where temperature tuning

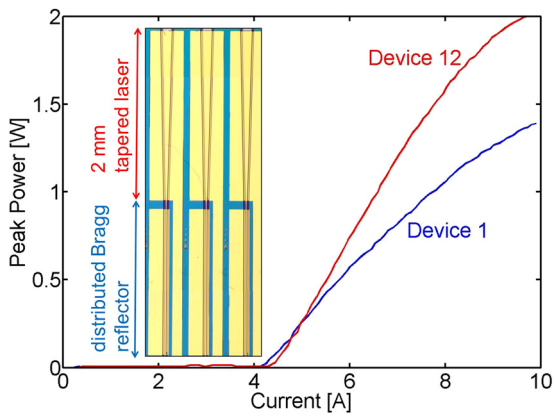

FIG. 1. Light-current characteristics at room temperature for two TO/DBR QCLs. The blue and red curves show the characteristics of the device with the lowest and highest slope efficiency on the chip, respectively. The inset presents a top view of the device layout for three chip elements. Note that the distributed Bragg reflector acting as a back mirror of the tapered laser cavity is electrically separated from the laser and left unpumped.

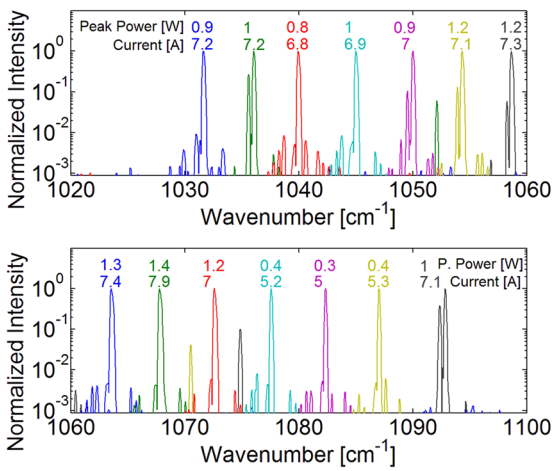

FIG. 2. Spectra and peak power. For each device, the spectrum at the given drive current is shown together with the respective peak power value, from device 1 emitting at low wavenumbers to device 14 lasing at high wavenumbers. For nine devices (1, 3, 4, 8, 9, 10, 11, 12, 13), single-mode operation with a side-mode suppression ratio of at least 20 dB was observed up to the given current value at a duty cycle of 0.04% and at room temperature.

over about $5\,cm^{-1}$ was used to cover the spectral gap between the design wavenumbers of adjacent array elements.

The peak power values shown in Fig. 2 were obtained by recording light/current (LI) characteristics at room temperature. For these measurements, the devices were driven by a pulse generator with a wider drive current range than the one used for measuring the spectra in Fig. 2. Due to the limitations of this high-power-source, 100-ns-long pulses had to be used, while the repetition rate was kept at 10 kHz. The individual devices exhibit a threshold current (density) between 4.2 A (3.5 kA/cm^2) and 4.6 A (3.8 kA/cm^2), with an average value of 4.3 A (3.6 kA/cm^2). The threshold current densities of the TO/DBR devices compare well to those reported in Refs. 14 and 15 for multi-mode TO QCLs fabricated from the same material, where values of 3.14 and 3.16 kA/cm^2 were found for a tapering angle of 1° and 2°, respectively.

The slope efficiencies at low currents found for the individual TO/DBR devices range from 340 mW/A to 460 mW/A, as seen in Fig. 1 which shows the LI characteristics of the two extreme devices. The curves of the other QCLs are spread between these extremes and are not shown. The slope efficiencies observed for the devices compare well to those reported in Ref. 14, where values of 315 mW/A and 300 mA/W were found for multi-mode TOs with sloped ridge walls and a tapering angle of 1° and 2°, respectively.

The LI characteristics show that the TO/DBR elements feature peak output powers of up to 2 W. To achieve high drive currents up to 9.9 A, a pulse length of 100 ns had to be employed due to limitations of the employed pulse generator, leading to significant self-heating and mode-hopping during the current pulse. Therefore, at these long driving pulses single-mode operation could only be confirmed for device 8, which exhibits single-mode operation with at least 20 dB SMSR up to a drive current of 9 A. The respective spectrum is shown in the inset of Fig. 3, exhibiting a SMSR ratio of 23 dB at a peak power of 1.6 W.

The figures of merit, in which tapered oscillators excel compared to broad-area-devices of rectangular design, are the beam quality and brightness. In order to quantitatively evaluate the beam quality of our TO/DBR QCLs, their far-field intensity distribution was measured in chip plane by a HgCdTe-detector mounted on a rotating arm at a distance of 18 cm from the device facet. For the far-field measurements, the devices were driven by 100 ns long pulses at a rate of 10 kHz. Figure 4 shows the angular in-plane intensity distribution for each of the devices at two different drive currents. At both currents all of the devices feature a single-lobed far-field distribution, with only minor contributions by higher-order lateral modes. At a current of 7 A, the full-width at half-maximum (FWHM) angle of the intensity distribution ranges from 6.4° to 7°, with an average value of 6.6°. The in-plane beam quality factor M^2 was deduced from the measured far-field characteristics by extracting the angular standard deviation of the intensity distribution σ_θ [rad] and using $M^2 = 4\pi\sigma_\theta\sigma_0/\lambda$ (Ref. 21), where λ is the emission wavelength and σ_0 the in-plane standard deviation of the spatial intensity distribution at the output facet. The latter was estimated by assuming a sinusoidal field distribution in the waveguide, giving $\sigma_0 = 0.18w$, where $w = 110\,\mu m$ is the width of the output facet. From the characteristics presented in Fig. 4, M^2-values between 1.3 and 1.6 were extracted for a current of 7 A, with a mean value of 1.5. Using the M^2-values, the peak brightness B of the elements was calculated from $B = P/(\lambda^2 M^2)$, where P is the peak power at the respective current. The peak brightness values achieved by the TO/DBR devices at 7 A range from 0.63 to 1 MW cm^{-2} sr^{-1}.

As seen in Fig. 4, an increase in the drive current results in an increase in the contribution of higher order lateral modes and/or in a broadening of the centre lobe for some devices (1, 2, 3, 5, and 6), while the far-field of others remains almost unchanged. At a current of 9.9 A, the observed M^2-values range from 1.44 to 2, with an average of 1.67, and are thus slightly higher than at 7 A. At 9.9 A, brightness values between 0.7 and 1.6 MW cm^{-2} sr^{-1} are achieved, with an average of 1.2 MW cm^{-2} sr^{-1}. Table I summarizes the figures measured at 9.9 A for each of the TO/DBR devices. The brightness range and M^2-values found for the TO/DBR QCLs compare well to the figures of merit reported in Ref. 14 for a multi-mode TO QCL, where a M^2-value range from 1.48 to 2.08 and a maximum peak

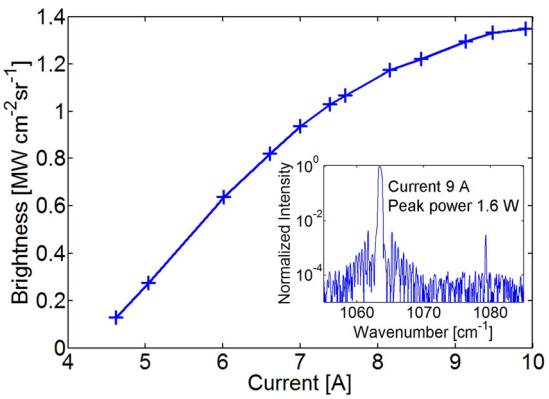

FIG. 3. Peak brightness as a function of drive current for device 8. This device exhibits single-mode operation up to high drive currents, as seen in the inset showing the spectrum at a drive current of 9 A and a peak power of 1.6 W.

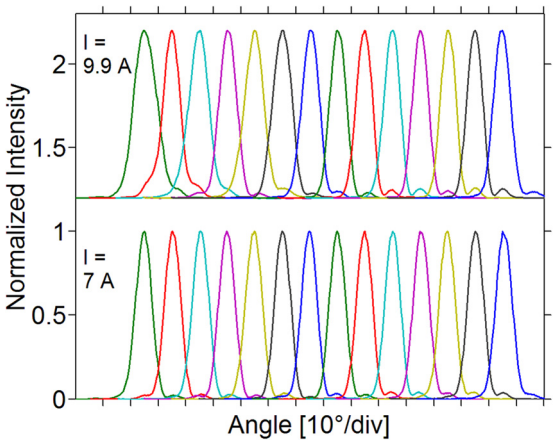

FIG. 4. Far-field intensity distribution. For each laser, the measured angular in-plane intensity distribution is shown for two different drive currents at a duty cycle of 0.1% and at room temperature. For a clear display, the curves for the individual devices are offset horizontally, while the curves measured at 9.9 A are offset vertically from those obtained at 7 A. The leftmost curves represent device 1 and the rightmost device 14.

TABLE I. Figures of merit at a drive current of 9.9 A for each device. Also shown are the emission wavenumbers and the peak power values available for single-mode operation with a side-mode suppression ratio of at least 20 dB.

		Figures of merit at 9.9 A			
Device No.	Wavenumber [cm^{-1}]	Peak power [W]	M^2	Peak brightness [$MW\,cm^{-2}\,sr^{-1}$]	Single mode peak power [W]
1	1031.6	1.4	2	0.7	0.9
2	1036.1	1.5	1.9	0.8	n/a
3	1040.0	1.5	1.9	0.9	0.8
4	1045.0	1.4	1.6	0.9	1
5	1049.5	1.4	2	0.8	n/a
6	1054.4	1.7	1.7	1.1	n/a
7	1058.7	1.8	1.6	1.3	n/a
8	1063.5	1.8	1.4	1.4	1.6
9	1067.8	1.8	1.5	1.4	1.4
10	1072.6	1.8	1.6	1.3	1.2
11	1077.6	1.9	1.4	1.5	0.4
12	1082.4	2	1.5	1.6	0.3
13	1087.1	1.9	1.5	1.5	0.4
14	1092.4	1.7	1.7	1.2	n/a

brightness of 1.4 $MW\,cm^{-2}\,sr^{-1}$ were found for a tapering angle of 1°. The comparison of the experimental results on our TO/DBR QCLs to the multi-mode tapered QCLs fabricated from the same material[14] confirms that excellent lateral mode filtering is achieved with the present device design.

Figure 3 shows the dependence of the peak brightness of device 8 on the drive current, as measured for a current pulse length and repetition rate of 100 ns and 10 kHz, respectively. For this device, the far-field distribution does not change significantly with the drive current, with M^2 values between 1.4 and 1.48 over the whole drive current range. The brightness characteristics therefore roughly follow the LI curve shape. Device 8 features impressive peak brightness values up to 1.35 $MW\,cm^{-2}\,sr^{-1}$ at a peak power of 1.8 W, with single-mode operation (>20 dB SMSR) up to a current of 9 A and a corresponding peak brightness of 1.28 $MW\,cm^{-2}\,sr^{-1}$.

In conclusion, we have demonstrated a series of tapered QCLs with a DBR back mirror, where each of the fourteen devices emits at a different wavelength between 9.2 and 9.7 μm. Each device achieves peak powers of at least 1.4 W, with values as high as 2 W. For nine devices single-mode operation (>20 dB SMSR) has been demonstrated, with six elements reaching peak power levels between 0.9 and 1.6 W. The devices further show excellent beam quality, with a narrow in-plane intensity distribution and high peak brightness values up to 1.6 $MW\,cm^{-2}\,sr^{-1}$. Our QCLs in TO/DBR configuration are highly suited for applications requiring single-mode operation and high beam quality at moderate power levels. For such applications, TO/DBRs as two-terminal devices pose significant advantages over MOPAs, as they allow a simple current drive setup and do not require the application of an anti-reflection coating.

The authors gratefully acknowledge the expert assistance of Jon Wilson for applying anti-reflection facet coatings and of Leo Missaggia for packaging devices. The authors acknowledge the Center for Nanoscale Systems (CNS) at Harvard University. Harvard CNS is a member of the National Nanotechnology Infrastructure Network (NNIN). This project received support from the Defense Threat Reduction Agency-Joint Science and Technology Office for Chemical and Biological Defense (Grant No. HDTRA1-10-1-0031-DOD). P. Rauter acknowledges support from the Austrian Science Fund (FWF): J 3092-N19. The Lincoln Laboratory portion of this work was sponsored by the Office of the Assistant Secretary of Defense for Research and Engineering under Air Force Contract No. FA8721-05-C-0002. The opinions, interpretations, conclusions, and recommendations are those of the authors and are not necessarily endorsed by the United States Government.

[1]J. Faist, F. Capasso, D. L. Sivco, C. Sirtori, A. L. Hutchinson, and A. Y. Cho, Science **264**, 553–556 (1994).
[2]C. Gmachl, F. Capasso, D. L. Sivco, and A. Y. Cho, Rep. Prog. Phys. **64**(11), 1533 (2001).
[3]Y. Yao, A. J. Hoffman, and C. Gmachl, Nat. Photonics **6**, 432 (2012).
[4]K. Degreif, S. Rademacher, P. Dasheva, F. Fuchs, S. Hugger, F. Schnürer, and W. Schweikert, Proc. SPIE **7945**, 79450P (2011).
[5]For a review on external cavity QCLs, see A. Hugi, R. Maulini, and J. Faist, Semicond. Sci. Technol. **25**, 083001 (2010).
[6]B. G. Lee, M. A. Belkin, C. Pflügl, L. Diehl, H. A. Zhang, R. M. Audet, J. MacArthur, D. P. Bour, S. W. Corzine, G. E. Höfler, and F. Capasso, IEEE J. Quantum Electron. **45**, 554 (2009).
[7]E. Mujagic, C. Schwarzer, Y. Yao, J. Chen, C. Gmachl, and G. Strasser, Appl. Phys. Lett. **98**, 141101 (2011).
[8]P. Rauter, S. Menzel, A. K. Goyal, B. Gokden, C. A. Wang, A. Sanchez, G. Turner, and F. Capasso, Appl. Phys. Lett. **101**, 261117 (2012).
[9]P. Rauter, S. Menzel, A. K. Goyal, C. A. Wang, A. Sanchez, G. Turner, and F. Capasso, Opt. Express **21**, 4518 (2013).
[10]T. Mansuripur, S. Menzel, R. Blanchard, L. Diehl, C. Pflugl, Y. Huang, J. H. Ryou, R. D. Dupuis, M. Loncar, and F. Capasso, Opt. Express **20**, 23339 (2012).
[11]S. Slivken, N. Bandyopadhyay, S. Tsao, S. Nida, Y. Bai, Q. Y. Lu, and M. Razeghi, Appl. Phys. Lett. **100**, 261112 (2012).
[12]P. Fuchs, J. Seufert, J. Koeth, J. Semmel, S. Hofling, L. Worschech, and A. Forchel, Appl. Phys. Lett. **97**, 181111 (2010).
[13]Y. Bai, S. Slivken, N. Bandyopadhyay, and M. Razeghi, Appl. Phys. Lett. **101**, 081106 (2012).

[14]B. Gokden, T. S. Mansuripur, R. Blanchard, C. Wang, A. Goyal, A. Sanchez-Rubio, G. Turner, and F. Capasso, Appl. Phys. Lett. **102**, 53503 (2013).
[15]C. A. Wang, A. K. Goyal, S. Menzel, D. R. Calawa, M. Spencer, M. K. Connors, D. McNulty, A. Sanchez, G. W. Turner, and F. Capasso, J. Cryst. Growth **370**, 212 (2013).
[16]B. Sumpf, K.-H. Hasler, P. Adamiec, F. Bugge, F. Dittmar, J. Fricke, H. Wenzel, M. Zorn, G. Erbert, and G. Tränkle, IEEE J. Sel. Top. Quantum **15**, 1009 (2009).
[17]L. Nahle, J. Semmel, W. Kaiser, S. Hofling, and A. Forchel, Appl. Phys. Lett. **91**, 181122 (2007).
[18]A. Wittmann, T. Gresch, E. Gini, L. Hvozdara, N. Hoyler, M. Giovannini, and J. Faist, IEEE J. Quantum Electron. **44**, 36 (2008).
[19]For a review article on tapered diode lasers, see J. N. Walpole, Opt. Quantum Electron. **28**, 623 (1996).
[20]B. G. Lee, M. A. Belkin, R. Audet, J. MacArthur, L. Diehl, C. Pflügl, and F. Capasso, Appl. Phys. Lett. **91**, 231101 (2007).
[21]G. Hatakoshi, Opt. Rev. **10**, 307 (2003).